Adsorption (2011) 17: 371–383
DOI 10.1007/s10450-011-9337-3

Adsorption equilibria of O_2, Ar, Kr and Xe on activated carbon and zeolites: single component and mixture data

R.E. Bazan · M. Bastos-Neto · A. Moeller · F. Dreisbach · R. Staudt

Received: 2 February 2010 / Accepted: 8 February 2011 / Published online: 23 February 2011

Abstract This work provides a set of experimental data on the adsorption of pure component, binary and ternary mixtures on activated carbon sample and two different zeolites at 303 K and moderate pressures (up to 10 bar for mixtures). Pure component data were measured by gravimetry and mixture data by volumetry coupled with chromatography. Results encourage more research on new materials and enhancement of adsorption-based separation processes with the proposed target.

Keywords Adsorption · Carbon · Zeolite · Noble gas · Oxygen · Argon · Krypton · Xenon · Separation

1 Introduction

Noble gases have very specific properties, such as the lack of chemical reactivity, low solubility, very low boiling and melting points and very low conductivity. These properties are key factors in lighting, medical, space and many other applications, for instance: to provide inert atmosphere for the production of air-sensitive compounds; in excimer lasers, which are commonly used in laser surgery and microfabrication; and as filler gases for the production of high-efficiency windows.

Argon, Krypton and Xenon are obtained from air through liquefaction, followed by fractional distillation—cryogenic separation process (The Linde Group 2009). Their natural abundances decrease as the atomic numbers increase and influence directly their prices on the gas market. Considering only the abundance and the difficulty in producing these noble gases, to give a notion of their prices on the market as an example, Argon can be 5 times more expensive than dry Nitrogen. Krypton is usually about 100 times more expensive than Argon and Xenon 10 times more than Krypton. The price per gram of Xenon can be comparable or even higher than the price of Gold.

During the last years adsorptive air separation processes have been increasingly applied with the purpose of improving the product purity with lower operational costs. However, the low efficiency of the adsorptive separation of Kr and Xe from air prevents the production of these noble gases simultaneously in adsorptive air separation units. The key aspect for the separation efficiency dwells in the adsorption selectivity—which depends on the used adsorbent material.

Literature reports regarding the adsorption of noble gases are scarce. Although some are concerned about the material adsorption properties and selectivity (Greathouse et al. 2009; Mueller et al. 2006), most of them are associated to other subjects like the study of structural and theoretical aspects of surface adsorption (Simonyan et al. 2001; Da Silva and Stampfl 2008); the treatment of nuclear off-gas (Munakata et al. 2003) and trace analysis for geophysical purposes (Marrocchi et al. 2005) for example. The purification of noble gases is also a problem of industrial interest and the development of an adsorption process for separation of O_2/Ar/Kr/Xe mixtures would increase productivity and the profit of adsorptive air separation units.

The objective of this work is to provide a set of experimental data on adsorption of noble gases and Oxygen and to encourage further research and development on this topic.

R.E. Bazan · M. Bastos-Neto · A. Moeller · R. Staudt (✉)
Institut für Nichtklassische Chemie e.V., University of Leipzig, Permoserstr. 15, 04318 Leipzig, Germany
e-mail: staudt@inc.uni-leipzig.de

F. Dreisbach
Rubotherm GmbH, Universitätstr. 142, 44799 Bochum, Germany

Table 1 Textural properties of the adsorbent samples

Property	B3	4AK	13X-K2
Specific surface area ($m^2\ g^{-1}$)[a]	778	[c]	479
Specific surface area ($m^2\ g^{-1}$)[b]	1012	477 [c,d]	640
Total pore volume ($cm^3\ g^{-1}$)	0.441	0.198 [c,d]	0.356
Average pore size (nm)	0.8	0.4	0.9
Form	Granular	Bead	Bead

[a]ISO 9277 (1995)

[b]Rouquerol et al. (1999)

[c]Could not be determined with N_2 at 77 K due to the low kinetics on the sample

[d]Evaluated with CO_2 isotherm at 273.15 K (Lowell et al. 2006)

Adsorption isotherms of O_2, Ar, Kr and Xe and some of their mixtures on activated carbon and zeolite samples were measured. Pure-component data were evaluated by gravimetry. Mixture data were obtained by volumetry coupled with chromatography.

2 Materials

Pure and mixture adsorption equilibrium of O_2, Ar, Kr and Xe were measured on three different samples at 30°C. One activated carbon (AC) SorboNorit B3 provided by the company Norit (The Netherlands) and two zeolites: Koestrolith 13X-K2 and Koestrolith 4AK supplied by CWK Chemiewerk Bad Köstritz GmbH (Germany). These samples were chosen due to their commercial availability and their different characteristics. The main textural properties of the carbon sample are summarized in Table 1.

3 Theory

3.1 Models for pure and multicomponent adsorption

Pure component data were handled with the Langmuir model in order to obtain parameters for further comparisons and to evaluate multicomponent adsorption (Do 1998).

The Ideal Adsorbed Solution Theory (IAST), originally proposed by Myers and Prausnitz (1965), was used for the analysis of multicomponent equilibrium adsorption. The model does not require data for mixtures and is thermodynamically consistent. Applying IAST requires the calculation of an integral equation to obtain the reduced spreading pressure. The binary data were evaluated by a procedure described by Do (1998) using the single component parameter set fitted with Langmuir model.

4 Experimental

4.1 Sample preparation

The specific mass loss for each adsorbent material during sample preparation was determined gravimetrically (Bazan et al. 2008).

The AC sample SorboNorit B3 (from 120 to 130 g) was regenerated at 373 K (2 K min^{-1}) under vacuum (10^{-7} bar) for 4 hours. The zeolites 13X-K2 and 4AK (∼230 g and ∼150 g, respectively) were regenerated at 673 K (heating rate of 1 K min^{-1}) under vacuum (10^{-7} bar) for 6 hours.

4.2 Sample characterization

The samples were analyzed for their textural characteristics by measuring N_2 isotherms at 77 K. The data handling for the calculation of BET specific surface area, pore volume and average pore size was accomplished in accordance with literature reports (ISO 9277 1995; Rouquerol et al. 1999).

4.3 Pure component data

The adsorption isotherms of pure components were measured gravimetrically using a high-precision magnetic suspension balance (Rubotherm, Germany). After the sample preparation the temperature was set to 303 K and pure gas was introduced in the sample cell up to a given pressure. The sample weight was observed and the equilibrium state was marked when no mass variation was detected. Each measurement at constant pressure corresponds to an experimental equilibrium point. The handling of the measured weight increase data in order to obtain excess adsorption isotherms can be found elsewhere (Dreisbach 1998; Herbst and Harting 2002; Dreisbach et al. 1999, 2002; Keller and Staudt 2005; Staudt et al. 1997; Do and Do 2003; Bastos-Neto et al. 2005).

4.4 Mixture data

Adsorption equilibrium data for mixtures were measured in a volumetric device, as shown in Fig. 1. It consists basically of two vessels with known volume (V_1) used to store a specific amount of the gas (or gases) that is opened to the adsorption chamber, with volume V_2, which contains the adsorbent material in analysis (volume V_S). Temperature and pressure conditions are controlled through sensors, whose characteristics are listed in Table 2.

All internal volumes were precisely determined by expansion experiments. The density of pure gases was obtained according to Schmidt and Wagner (1985), Tegeler et al. (1999) and Lemmon and Span (2006). The density of

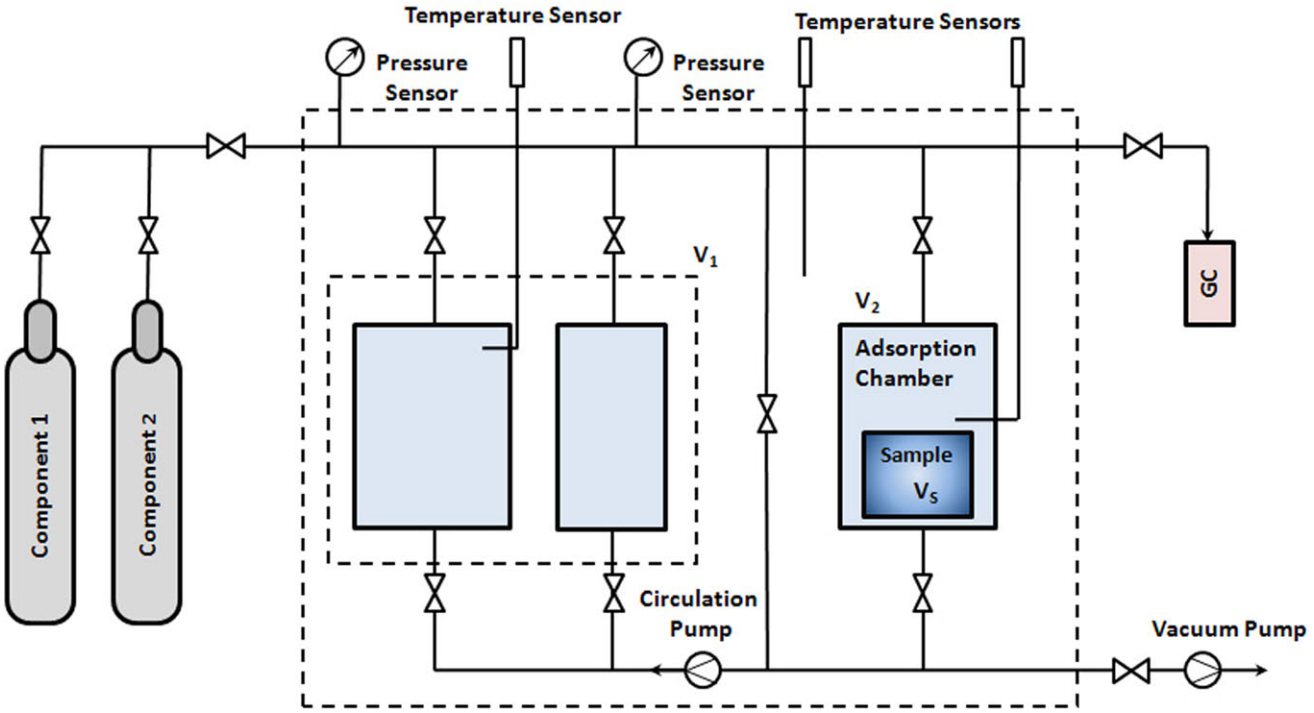

Fig. 1 Scheme of the volumetric apparatus

Table 2 Sensors specifications

Sensor	Specification	Accuracy
Pressure	0.8 . . . 1, 2 bar abs. 0 → 323 K	±0.08%
	0 . . . 25 bar 263 → 353 K	±0.03%
	0 . . . 160 bar 263 → 353 K	±0.09%
Temperature	223 → 673 K	±0.1 K
GC-HP 5980 Detector: TCD	343 K 303 → 323 K, 373 K 4.5 ml min^{-1}	±0.05% (mol)

mixtures, which are also dependent on the pressure, temperature and composition were evaluated using the Redlich-Kwong-Soave equation of state (Sandler 1999). The binary interaction coefficient was set zero and the (pseudo)critical temperature of the mixture was evaluated according to Reid et al. (1987).

The mixture preparation was carried out using the whole volume V_1. The desired partial pressures were previously estimated for the given temperature, considering the volume needed for GC composition analysis. Then, each component was stepwise added to the system following the order of increasing component concentration (Bazan et al. 2008).

After preparation, the gas mixture was expanded to the adsorption chamber and, with the aid of the circulation pump, the system was kept homogenized. The adsorption equilibrium was reached within 3 hours, when no pressure variation was detected (Bazan et al. 2008) and the composition of the gas phase, monitored with GC analyses, remained constant after at least three measurements.

4.5 Selectivity

The selectivity (S_{AB}) of the component A in a mixture A/B was calculated from the ratios of gas mole fractions in the gas phase (y) and in the adsorbed phase (x) according to the following equation (Greathouse et al. 2009):

$$S_{AB} = \frac{x_A y_B}{x_B y_A} \tag{1}$$

5 Results and discussion

This work is focused on the experimental determination of partial loadings from measurements of multicomponent adsorption employing a volumetric/chromatographic method following the guidelines reported by Talu (1998). The partial loadings were determined directly through mass balances from an analysis of the composition of the gas mixture before and after adsorption equilibrium.

5.1 Pure component

The obtained experimental data with the respective Langmuir fit are presented in Fig. 2, Tables 3 and 4.

From those data it is possible to observe that even though the samples have different polarities, pore sizes, specific surface areas and pore volumes, the isotherm profiles are qualitatively the same for all three adsorbents. This indicates that the adsorptives' thermophysical properties play the major role on the equilibrium of adsorption. However it was detected that the zeolite Koestrolith 4AK adsorbs much less than the other samples, certainly due to its low pore volume. Furthermore, the low kinetics related to the small pore size leads to extremely long times for the equilibrium to be reached.

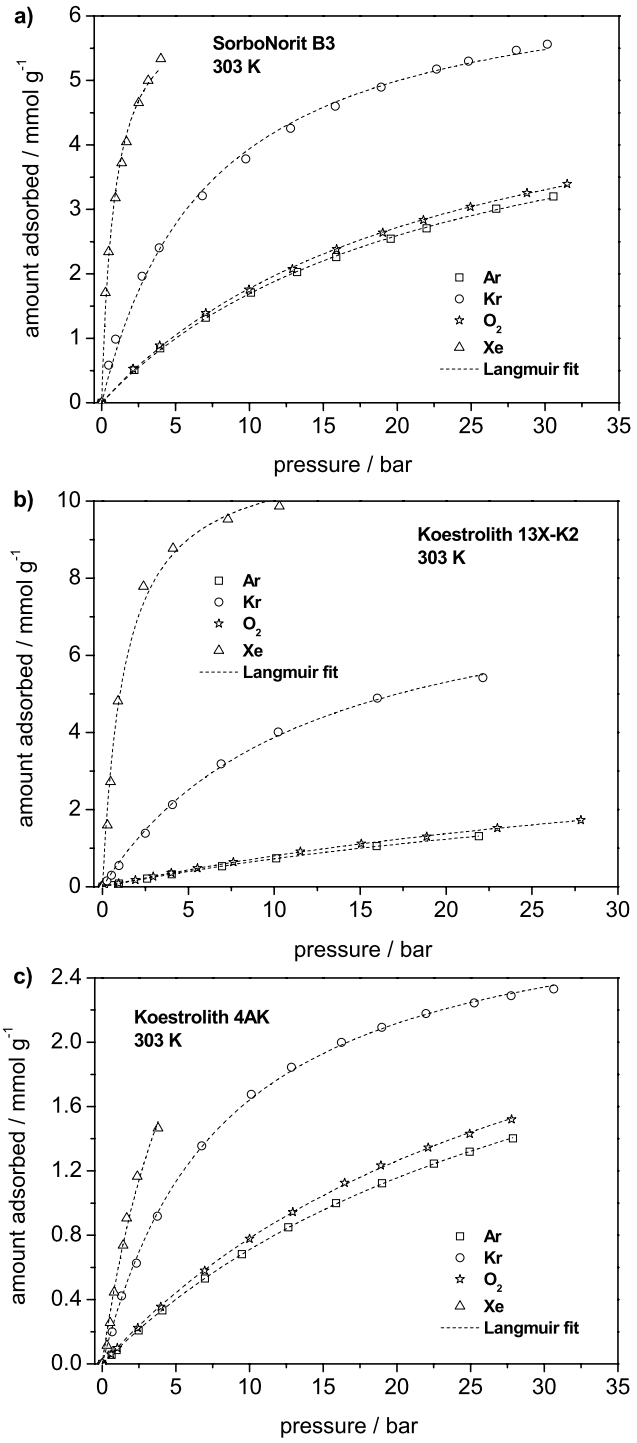

Fig. 2 Adsorption isotherms of Ar, Kr, Xe and O_2 on (**a**) SorboNorit B3; (**b**) Koestrolith 13X-K2 and (**c**) Koestrolith 4AK

In every case Xe was the most strongly adsorbed, followed by Kr, then O_2 and Ar. The similarity between O_2 and Ar adsorption by each adsorbent is very remarkable.

For a better sample comparison Fig. 3 was created with the plots of each gas using the Langmuir model fits at the experimental pressure ranges.

Comparing the Langmuir fits with data reported on literature, it is possible to conclude that the results presented in this work are in conformity with the order of magnitude.

One can note that the adsorption of Ar is also quantitatively very similar to the adsorption of O_2. For both gases the AC SorboNorit B3 shows much better performance than the zeolites. Additionally, the sample SorboNorit B3 presented adsorption capacity for Ar similar to the Ag-ETS-10 reported by Ansón et al. (2008) and the IRMOF-1 reported by Greathouse et al. (2009) for pressures up to 10 bar. Adsorption capacities of O_2 on our zeolites are comparable to literature data, which presented performance inferior to the SorboNorit B3.

Data on Kr adsorption are also in good agreement with literature reports. The 5A-CMS studied by Mahajan and Walker (1969) showed however, a more improved adsorption capacity for Kr in comparison with our samples. AC SorboNorit B3 and Koestrolith 13X-K2 compete to each other for the best adsorption capacity. The carbon shows a slightly better performance than the zeolite up to ca. 12 bar, when both isotherms cross each other and the last one turns to show higher adsorption capacity.

In the case of Xe, the zeolite Koestrolith 13X-K2 clearly showed the best adsorption capacity followed by our carbon sample. The poor adsorption performance of the sample Koestrolith 4AK indicates that its textural characteristics may not be favorable for the adsorption of this gas.

Textural characteristics are known to play an important role on the adsorption properties (Bastos-Neto et al. 2007). By comparing only these characteristics displayed in Table 1, it is possible to understand why the sample Koestrolith 4AK, for example, presented the least favorable results with all gases since it is expected that lower pore volumes tend to lead to inferior adsorption capacities. Additionally, the sample presents the smallest average pore size, which consists of a barrier for the diffusion of relatively bigger molecules such as Xe.

Table 3 Experimental pure component isotherm data

Ar		Kr		O_2		Xe	
Pressure [bar]	Adsorbed amount [mmol/g]	Pressure [bar]	Adsorbed amount [mmol/g]	Pressure [bar]	Adsorbed amount [mmol/g]	Pressure [bar]	Adsorbed amount [mmol/g]
SorboNorit B3							
0.000	0.0000	0.000	0.000	0.000	0.000	0.000	0.000
2.222	0.5097	0.472	0.583	2.123	0.527	0.269	1.705
3.967	0.8468	0.949	0.985	3.934	0.888	0.485	2.340
7.057	1.3206	2.743	1.961	7.057	1.388	0.941	3.174
10.116	1.7091	3.910	2.404	9.966	1.756	1.367	3.721
13.235	2.0278	6.817	3.210	12.905	2.075	1.691	4.047
15.874	2.2595	9.760	3.782	15.904	2.384	2.510	4.654
19.563	2.5423	12.790	4.256	19.026	2.639	3.158	4.995
21.993	2.7059	15.820	4.600	21.777	2.834	4.003	5.335
26.701	3.0088	18.910	4.895	24.962	3.038		
30.570	3.2005	22.660	5.175	28.774	3.252		
		24.820	5.298	31.494	3.392		
		28.060	5.467				
		30.160	5.562				
Koestrolith 13X-K2							
0.000	0.0000	0.000	0.0000	0.000	0.000	0.000	0.0000
0.102	0.0089	0.103	0.0596	0.943	0.086	0.283	1.5984
0.263	0.0223	0.260	0.1501	1.923	0.175	0.470	2.7185
0.503	0.0420	0.518	0.2980	2.952	0.264	0.899	4.8124
0.962	0.0802	0.962	0.5505	4.008	0.358	2.393	7.7858
2.603	0.2117	2.492	1.3843	5.535	0.479	4.117	8.7701
4.027	0.3205	4.072	2.1287	7.617	0.639	7.297	9.5284
6.967	0.5330	6.907	3.1875	11.514	0.910	10.296	9.8626
10.116	0.7372	10.236	4.0112	15.060	1.116		
15.964	1.0537	15.994	4.8875	18.870	1.297		
21.903	1.3083	22.143	5.4221	22.980	1.519		
				27.840	1.727		
Koestrolith 4AK							
0.000	0.0000	0.000	0.0000	0.000	0.0000	0.000	0.0000
0.643	0.0565	0.676	0.1994	0.613	0.0588	0.319	0.1132
0.988	0.0859	1.321	0.4228	1.027	0.0981	0.544	0.2550
2.485	0.2083	2.323	0.6257	2.422	0.2234	0.820	0.4448
4.084	0.3320	3.748	0.9180	3.982	0.3548	1.420	0.7363
6.976	0.5308	6.760	1.3552	6.955	0.5798	1.666	0.9048
9.490	0.6818	10.120	1.6762	10.000	0.7775	2.383	1.1646
12.640	0.8490	12.850	1.8449	12.940	0.9431	3.802	1.4658
15.880	0.9989	16.240	1.9985	16.450	1.1261		
19.000	1.1228	18.970	2.0927	18.910	1.2330		
22.510	1.2445	21.970	2.1779	22.120	1.3448		
24.940	1.3196	25.240	2.2441	24.940	1.4302		
27.880	1.4015	27.760	2.2897	27.790	1.5196		
		30.640	2.3317				

Table 4 Langmuir fit parameters for the single component isotherms

q_{max}: specific saturation adsorption capacity in the Langmuir isotherm [mmol g^{-1}]

b: Langmuir adsorption constant [bar^{-1}]

Sample	Ar		Kr		O_2		Xe	
	q_{max}	b	q_{max}	b	q_{max}	b	q_{max}	b
SorboNorit B3	5.555	0.044	6.811	0.137	5.817	0.044	6.335	1.135
Koestrolith 13X-K2	4.118	0.021	8.430	0.085	4.839	0.020	11.344	0.773
Koestrolith 4AK	3.106	0.030	2.981	0.122	3.308	0.031	3.918	0.165

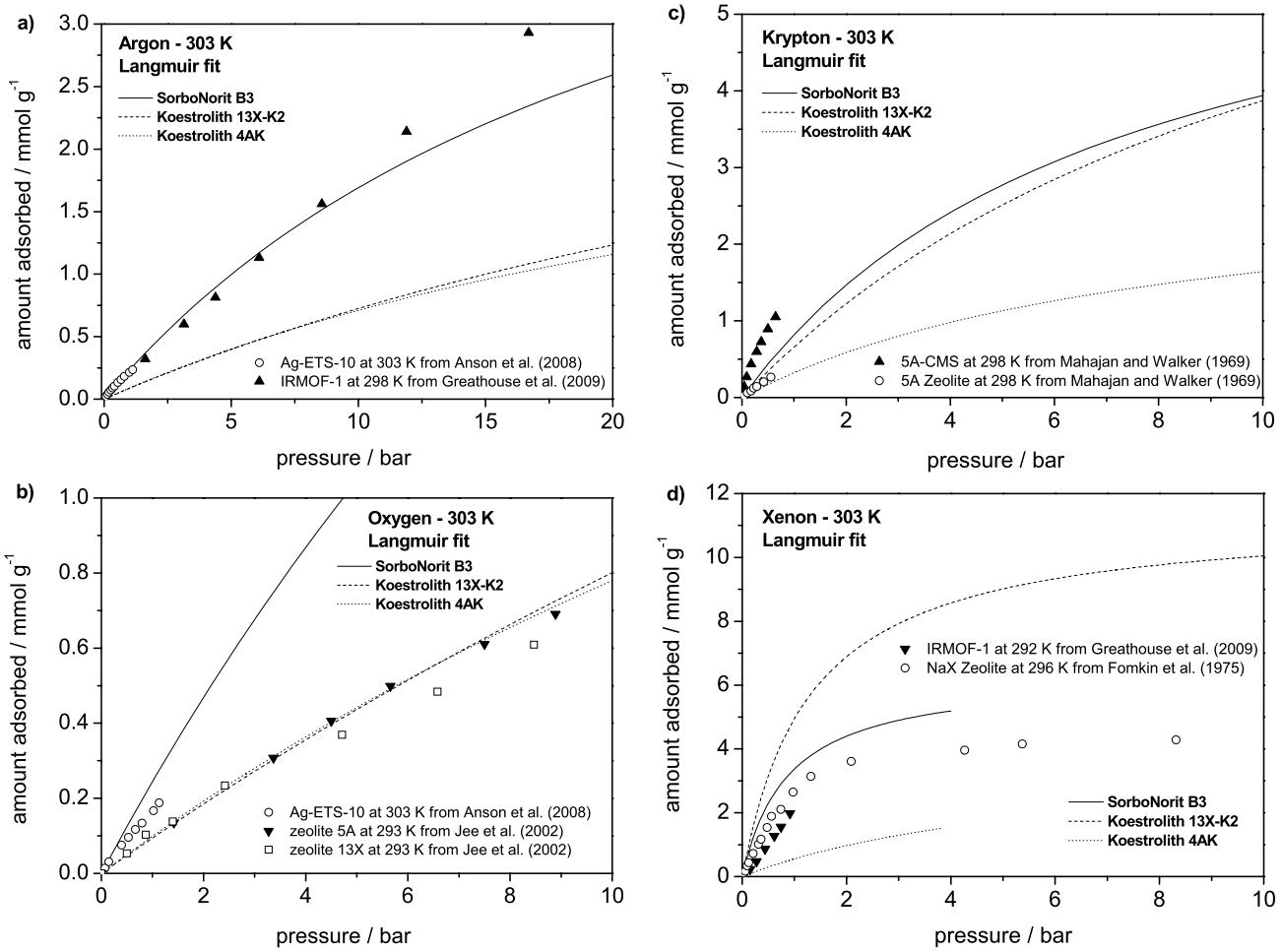

Fig. 3 Adsorption isotherms on the three samples. (**a**) Argon; (**b**) Oxygen; (**c**) Krypton (Jee et al. 2002) and (**d**) Xenon (Fomkin et al. 1975)

It is important to note that all pure component isotherms presented Type-I feature, which is typical for the adsorption mechanism of supercritical gases in low pressure ranges. The sequence of adsorption preference and capacity of the studied gases for all adsorbents is directly proportional to the sequence of the critical temperatures of the gases. Referring to Table 5, one can conclude that the higher the critical temperature, the larger the amount adsorbed independently on the studied adsorbent material. Another expected consequence of working with adsorption of supercritical fluids is that for a given gas, the larger the specific surface area, the higher the adsorption capacities are reached. Such behavior is also observed from the data reported in Table 1.

Intriguingly, with only those arguments it is not possible to elucidate the competition between Koestrolith 13X-K2 and SorboNorit B3. Their average pore sizes are practically the same and apparently play no important role on the differential adsorption. The carbon has higher specific surface area and total pore volume and this explains the higher uptakes of Ar and O_2. With Kr and Xe, for which the experimental conditions are closer to the critical temperature, another factor significantly interferes on the adsorption affinity of the zeolite. Carbons are known to be apolar as zeo-

Table 5 Some properties of the used gases

Gas	Van-der Waals radii[a] [nm]	Heat of evaporation [kJ mol^{-1}]	Boiling point [K]	Critical temperature [K]	Polarizability $\alpha/10^{-30}$ [m^3]
O_2	0.152	6.8[b]	90.2	154.6	1.541[c]
Ar	0.188	6.447	87.3	150.8	1.642[d]
Kr	0.202	9.029	119.9	209.4	2.486[d]
Xe	0.216	12.636	165.1	289.7	4.047[d]

[a]Bondi (1964)

[b]Dobrinski et al. (2003)

[c]Hettema et al. (1994)

[d]Pershina et al. (2008)

lites polar and the reason for the overcoming performance of Koestrolith 13X-K2 might be attributed to an electrostatic related factor.

The polarizabilities (Table 5) from Ar and O_2 differ about 6% from each other and are not supposed to considerably influence the adsorption by all samples. This difference is raised to more than 50% for Kr, comparing with Ar and O_2. As a result of the pressure (and consequently density) increase, a growing number of Kr molecules would be affected by the higher polarity of the zeolite surface turning them more susceptible to polarization. Taking into account the affinity of species from the same nature (polar or apolar), those polarized molecules would be more easily attracted by the zeolite rather than by the carbon sample. Xe has a polarizability value about 60% higher than Kr, therefore its probability to be attracted by a polar sur-

Table 6 Binary adsorption data on SorboNorit B3

Mixture	y_A	x_A		n_A		N		P	S_{AB}
		exp	IAST	exp	IAST	exp	IAST		
A: Kr	0.055	0.224	0.188	0.429	0.322	1.917	1.710	8.65	4.95
B: Ar	0.030	0.173	0.110	0.318	0.178	1.838	1.622	8.61	6.77
A: Xe	0.014	0.331	0.307	0.675	0.585	2.040	1.902	8.34	34.44
B: Ar	0.006	0.180	0.160	0.337	0.271	1.875	1.698	8.52	36.33
A: Xe	0.021	0.167	0.140	0.542	0.475	3.245	3.391	6.40	9.49
B: Kr	0.008	0.070	0.057	0.224	0.189	3.214	3.298	6.52	9.84
A: O_2	0.905	0.904	0.910	1.485	1.429	1.714	1.570	8.48	1.00
B: Ar	0.950	0.952	0.953	1.616	1.523	1.697	1.597	8.66	1.05
A: Kr	0.060	0.221	0.195	0.423	0.345	1.912	1.775	8.53	4.48
B: O_2	0.025	0.128	0.088	0.233	0.148	1.816	1.671	8.58	5.75
A: Xe	0.011	0.294	0.245	0.577	0.459	1.965	1.871	8.25	37.39
B: O_2	0.006	0.168	0.153	0.311	0.274	1.853	1.789	8.67	36.54

P: total pressure [bar]

N: total adsorbed amount [mmol g^{-1}], n_A: partial adsorbed amount [mmol g^{-1}]

exp: experimental data

Table 7 Binary adsorption data on Koestrolith 13X-K2

Mixture	y_A	x_A		n_A		N		P	S_{AB}
		exp	IAST	exp	IAST	exp	IAST		
A: Kr	0.060	0.274	0.351	0.091	0.135	0.333	0.386	3.33	5.91
B: Ar	0.030	0.146	0.207	0.046	0.069	0.317	0.335	3.38	5.54
A: Xe	0.020	0.371	0.805	0.154	0.594	0.413	0.738	3.22	28.94
B: Ar	0.010	0.216	0.560	0.077	0.299	0.359	0.534	3.36	27.21
A: Xe	0.035	0.188	0.325	0.141	0.600	0.747	1.847	2.32	6.42
B: Kr	0.016	0.101	0.181	0.075	0.307	0.742	1.697	2.49	6.74
A: O_2	0.900	0.901	0.911	0.284	0.275	0.315	0.301	3.38	1.01
B: Ar	0.949	0.951	0.957	0.302	0.293	0.317	0.306	3.42	1.04
A: Kr	0.064	0.245	0.349	0.087	0.146	0.354	0.418	3.33	4.73
B: O_2	0.032	0.128	0.205	0.044	0.075	0.340	0.365	3.39	4.42
A: Xe	0.023	0.349	0.729	0.149	0.609	0.427	0.836	3.17	22.76
B: O_2	0.012	0.200	0.573	0.074	0.348	0.369	0.608	3.34	20.32

P: total pressure [bar]

N: total adsorbed amount [mmol g^{-1}], n_A: partial adsorbed amount [mmol g^{-1}]

exp: experimental data

Table 8 Binary adsorption data on Koestrolith 4AK

Mixture	y_A	x_A		n_A		N		P	S_{AB}
		exp	IAST	exp	IAST	exp	IAST		
A: Kr	0.075	0.259	0.243	0.234	0.197	0.903	0.813	9.81	4.31
B: Ar	0.040	0.161	0.141	0.131	0.108	0.809	0.761	9.80	4.62
A: Xe	0.075	0.248	0.374	0.212	0.355	0.855	0.951	9.92	4.07
B: Ar	0.028	0.171	0.173	0.143	0.138	0.836	0.800	9.89	7.17
A: O_2	0.900	0.900	0.910	0.739	0.696	0.821	0.764	9.85	1.00
B: Ar	0.950	0.950	0.956	0.770	0.738	0.811	0.772	9.92	1.00
A: Kr	0.068	0.224	0.205	0.213	0.176	0.949	0.858	9.73	3.96
B: O_2	0.035	0.139	0.114	0.120	0.092	0.865	0.811	9.70	4.44

P: total pressure [bar]
N: total adsorbed amount [mmol g^{-1}], n_A: partial adsorbed amount [mmol g^{-1}]
exp: experimental data

face is much higher and that can be the reason for the better adsorption by Koestrolith 13X-K2 in comparison with the SorboNorit B3.

5.2 Mixtures

All measured binary data are summarized in Table 6 (SorboNorit B3), Table 7 (Koestrolith 13X-K2) and Table 8 (Koestrolith 4AK). The experimental error for mixture data is expected to be about 5% (±2.5%) and depends mainly on the determination of gas phase composition (chromatography).

The binary mixture Ar/O_2 deserves a special attention due to the technological challenges involved on the separation of both species. The similarity between the adsorption of O_2 and Ar could be verified before. Additionally, in Table 5, we can see that argon and oxygen have other similar properties like molecular size, boiling point as well as adsorption affinity, which make them very hard to be separated. Developments on this subject are desirable for both oxygen purification and argon production processes.

A graph of the Ar/O_2 system was plotted in Fig. 4 for the zeolite Koestrolith 13X-K2. The experimental data at two different equilibrium concentrations are compared with the curve generated by the IAST model at an average value of the experimental pressure conditions, using the Langmuir fit parameters for pure component equilibrium. Figure 4(a) presents the amount adsorbed against the Argon gas phase equilibrium concentration. The similarity is here confirmed by the symmetry of the lines. Good agreement between model and experiment can be observed. Figure 4(b) exhibits the x–y diagram for the same system, indicating almost linear relationship between gas-phase and adsorbed-phase concentrations in equilibrium. The selectivity for O_2 in this system was 1.01 at $y_{Ar} = 0.1$ and 1.04 at $y_{Ar} = 0.05$, which indicates slightly preferable adsorption of Oxygen over Argon.

Rege and Yang (2000) brought up the problem of separating Ar/O_2 by PSA and concluded that a kinetically controlled process should be more feasible and not energy-intensive like cryogenic distillation/adsorption. Jin et al. (2006) made a further investigation on kinetically controlled

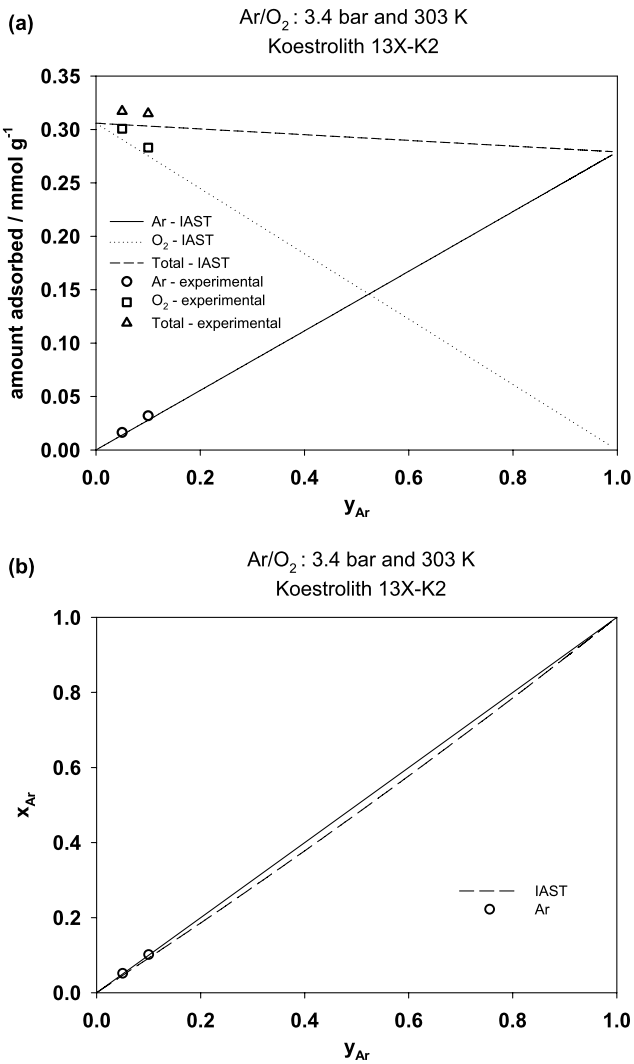

Fig. 4 Binary adsorption of Argon and Oxygen. (**a**) Adsorbed amount versus Ar concentration in the gas phase and (**b**) x–y diagram

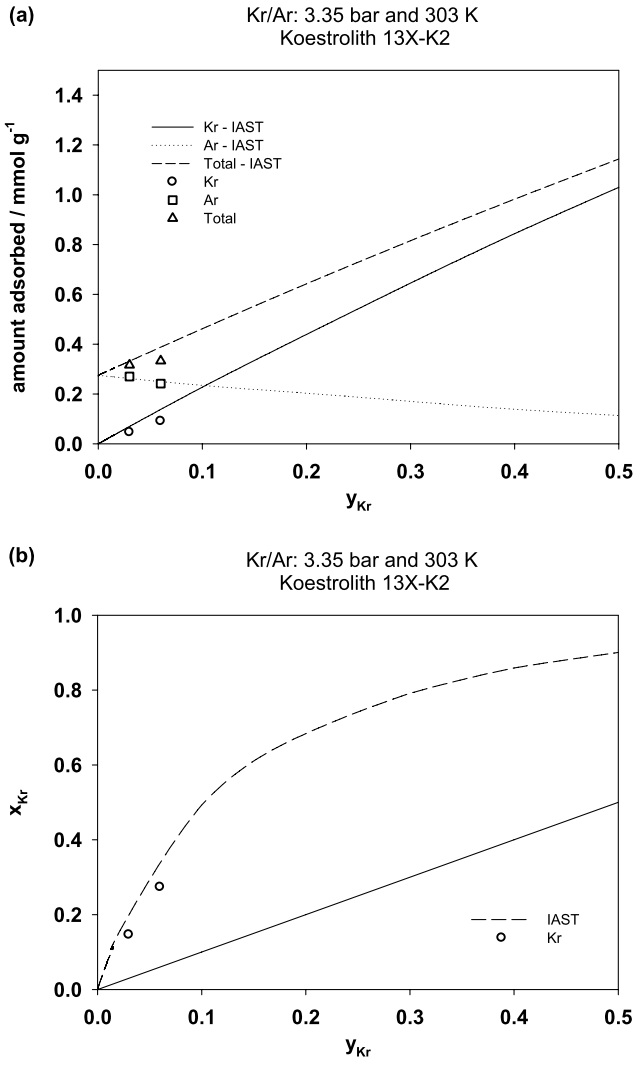

Fig. 5 Binary adsorption of Argon and Krypton. (**a**) Adsorbed amount versus Kr concentration in the gas phase and (**b**) $x-y$ diagram

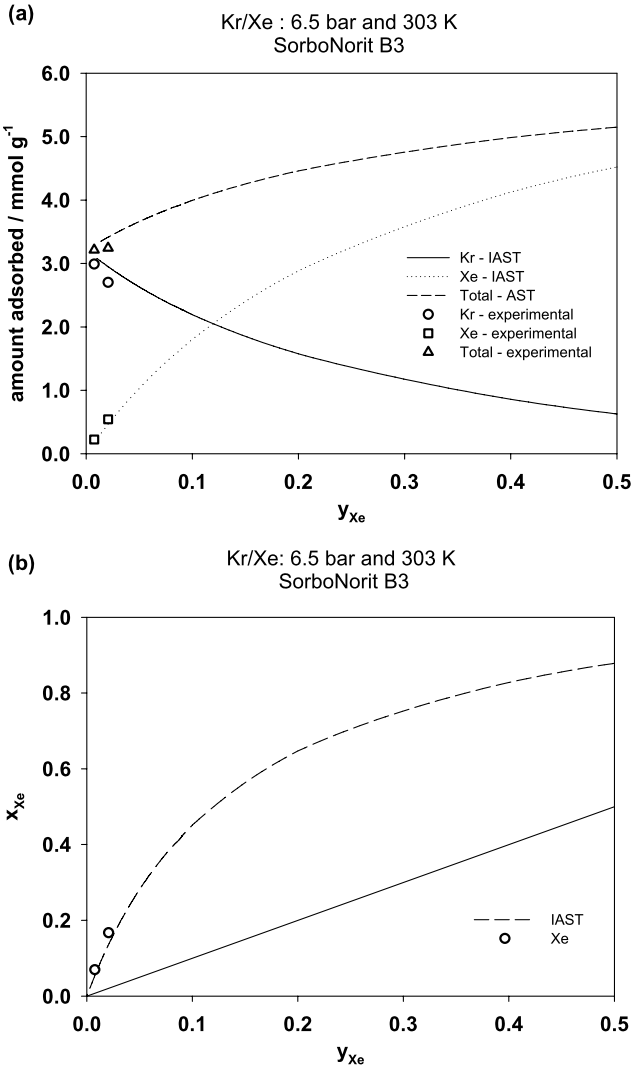

Fig. 6 Binary adsorption of Krypton and Xenon. (**a**) Adsorbed amount versus Xe concentration in the gas phase and (**b**) $x-y$ diagram

Oxygen-Argon separation for Argon production with different adsorbents and found out that such process is significantly affected by the operating conditions.

Ansón et al. (2008) carried out adsorption measurements of Ar, O_2 and N_2 in silver exchanged zeolites, which demonstrated selectivity for Argon over Oxygen. The authors suggested that those adsorbents could be useful for the production of high purity Oxygen (>99%) from a previously enriched Oxygen stream (from PSA air separation) containing approximately 95% O_2 and 5% Ar.

Either by kinetic or equilibrium controlled processes, this matter should be dealt with more research and development on new materials capable of efficiently make use of the small differences on the physical properties of both species to potentialize the separation.

Similar plots for the mixture Ar/Kr on the zeolite Koestrolith 13X-K2 are presented on Fig. 5. The preferential adsorption for Kr may be verified in both plots and the total amount adsorbed increases with the concentration of Kr on the gas phase. Satisfactory matching is also found between experimental data and IAST predictions, especially for Ar. The slight discrepancies are attributed to the IAST input data of the pure component equilibrium, which corresponds to the Langmuir fit parameters. In this case, one can infer that the description of the experimental results for Kr by the Langmuir model is inadequate.

The binary mixture Kr/Xe in SorboNorit B3 is presented in Fig. 6. The relevance of studying this mixture is regarded by the high commercial value of xenon and its increasing demand for current applications. Figure 6(a) shows also good agreement between model (IAST) and experimental data. The total amount adsorbed tends to increase with the Xe concentration. The $x-y$ diagram in Fig. 6(b) reveals the bigger affinity for Xe in comparison with Kr. The selectivity for Xe reaches 9.49 at $y_{Xe} = 0.02$ and 9.84 at $y_{Xe} = 0.008$.

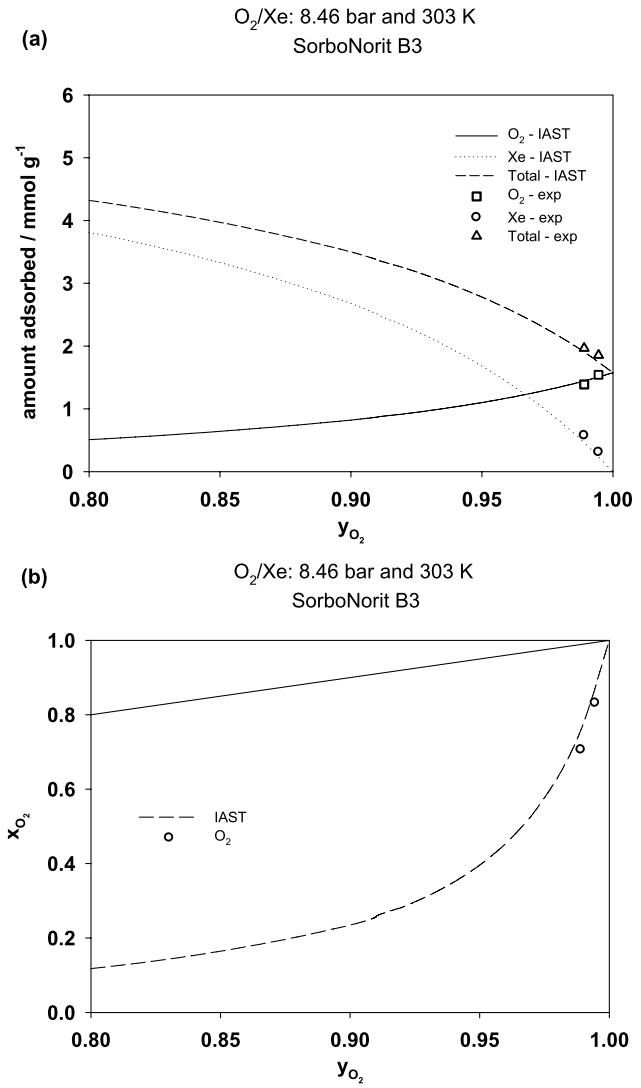

Fig. 7 Binary adsorption of Oxygen and Xenon. (**a**) Adsorbed amount versus O_2 concentration in the gas phase and (**b**) $x-y$ diagram

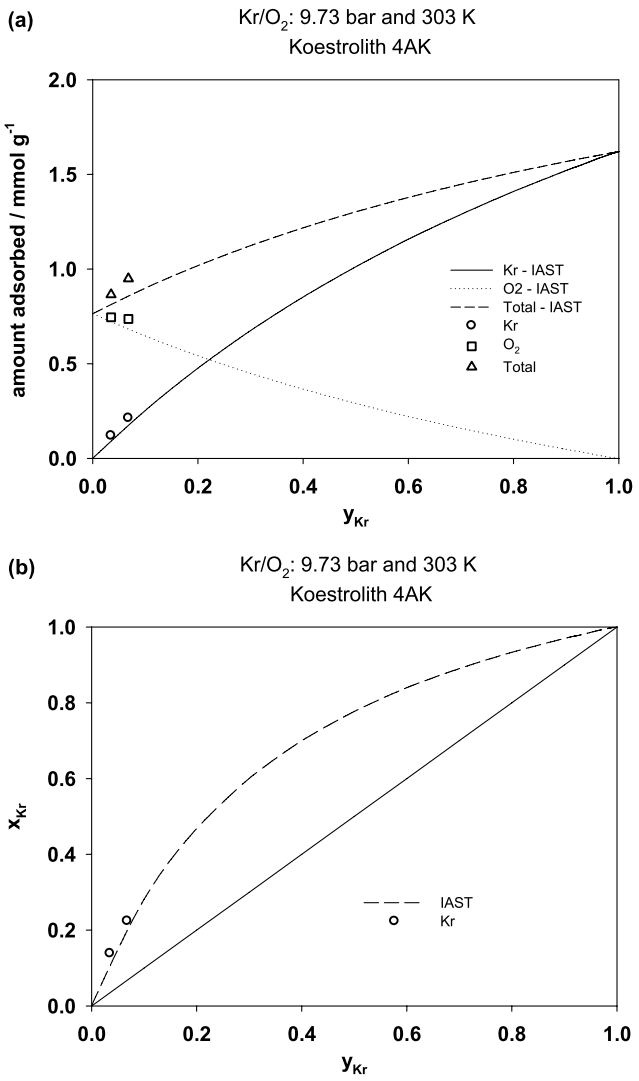

Fig. 8 Binary adsorption of Krypton and Oxygen. (**a**) Adsorbed amount versus Kr concentration in the gas phase and (**b**) $x-y$ diagram

Those values are notably larger than the ones calculated by Greathouse et al. (2009) with GCMC simulations of gas adsorption by IRMOF-1.

As mentioned before, both species Kr and Xe are very important for many applications today. Several materials could fulfill the requirements to separate them as they can be more easily adsorbed. The problem, in the viewpoint of production, is their very low concentration in the main source (air). Therefore, adsorption plays important role on the development of energy-efficient processes.

Other mixtures of industrial interest are the Xe/O_2 and Kr/O_2. The corresponding binary data are plotted in Fig. 7 for the AC SorboNorit B3 and Fig. 8 for the zeolite Koestrolith 4AK, respectively. The plots reveal the preferential adsorption of Xe and Kr over O_2. IAST predictions were very accurate for the first mixture but less for the last, evidencing imprecision on the description of the pure component isotherms on the Koestrolith 4AK.

Further comparisons between experimental data and IAST predictions for the binary mixtures might be observed directly from Tables 6–8.

The data corresponding to the ternary mixtures are presented in Table 9 for the AC sample and Table 10 for the zeolite Koestrolith 4AK. For a better visualization of the adsorption equilibrium, Figs. 9 and 10 were plotted for SorboNorit B3 and Fig. 11 for Koestrolith 4AK.

The ternary diagrams indicate the direction, in which there is preferable adsorption. Each point in those graphs represents the coordinates of the concentration of each species in a given mixture. Circles are used for the concentration in the gas phase and triangles for the concentration in the adsorbed phase. Stars indicate the IAST predictions for the concentration in the adsorbed phase. The line that

Table 9 Ternary adsorption data on SorboNorit B3

Mixture	i	y_i	x_i		n_i		N		P
			exp	IAST	exp	IAST	exp	IAST	
O_2/Ar/Kr	Kr	0.030	0.111	0.105	0.206	0.176	1.849	1.682	8.59
	Ar	0.100	0.100	0.088	0.185	0.148			
	O_2	0.870	0.789	0.807	1.459	1.359			
O_2/Ar/Xe	Xe	0.007	0.176	0.169	0.331	0.298	1.886	1.766	8.35
	Ar	0.109	0.074	0.086	0.139	0.153			
	O_2	0.884	0.751	0.745	1.416	1.315			
O_2/Kr/Xe	Xe	0.006	0.142	0.125	0.289	0.245	2.038	1.963	8.33
	Kr	0.076	0.215	0.209	0.439	0.409			
	O_2	0.918	0.643	0.666	1.309	1.308			
Ar/Kr/Xe	Xe	0.007	0.153	0.150	0.307	0.289	2.008	1.931	8.42
	Kr	0.072	0.222	0.203	0.446	0.392			
	Ar	0.921	0.625	0.647	1.256	1.251			

P: total pressure [bar]
N: total adsorbed amount [mmol g^{-1}], n_i: partial adsorbed amount [mmol g^{-1}]
exp: experimental data

Table 10 Ternary adsorption data on Koestrolith 4AK

Mixture	i	y_i	x_i		n_i		N		P
			exp	IAST	exp	IAST	exp	IAST	
O_2/Ar/Kr	Kr	0.038	0.136	0.120	0.108	0.098	0.797	0.811	9.77
	Ar	0.112	0.058	0.093	0.046	0.075			
	O_2	0.851	0.806	0.787	0.643	0.638			
O_2/Ar/Xe	Xe	0.035	0.150	0.188	0.126	0.163	0.837	0.870	9.80
	Ar	0.108	0.048	0.082	0.040	0.071			
	O_2	0.858	0.801	0.730	0.671	0.636			

P: total pressure [bar]
N: total adsorbed amount [mmol g^{-1}], n_i: partial adsorbed amount [mmol g^{-1}]
exp: experimental data

connects a circle (origin) to a triangle (end) symbolizes the equilibrium of adsorption and points toward the species with more adsorption affinity. The longer the line is, the higher the affinity.

The blank symbols representing the mixture Ar/Kr/Xe in Fig. 9 show the AC sample's high preferential adsorption of Xe and less significantly of Kr as their concentrations in the adsorbed phase are considerably increased when compared to the gas phase while the concentration of Ar is notably reduced. The filled symbols corresponding to the mixture Ar/O_2/Kr in the same plot also shows a small trend for O_2 and even more for Kr. As visible in Table 9, the concentration of Ar is practically the same in the gas and in the adsorbed phase, revealing its weaker adsorption by SorboNorit B3. Figure 10 also displays the preferential adsorption for Xe in both mixtures, confirming previous comments about its properties. In both figures, the matching between experiments and IAST predictions was exceptionally good.

Similar comments can be used for the mixtures presented in Fig. 11. In both cases there is a "decrease in the concentration" of Ar and O_2 as Kr or Xe exhibit better adsorption capacities, although O_2 shows a slighter reduction.

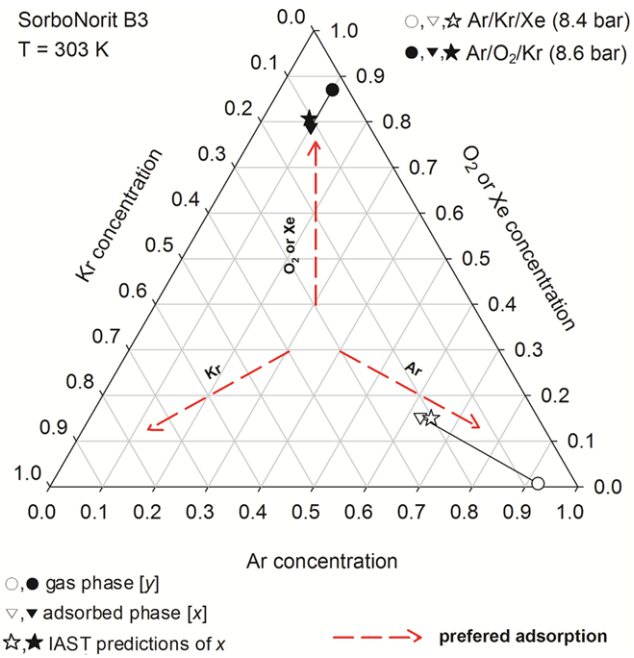

Fig. 9 Ternary diagram for adsorption of Ar/O_2/Kr and Ar/Kr/Xe on AC SorboNorit B3 at 303 K

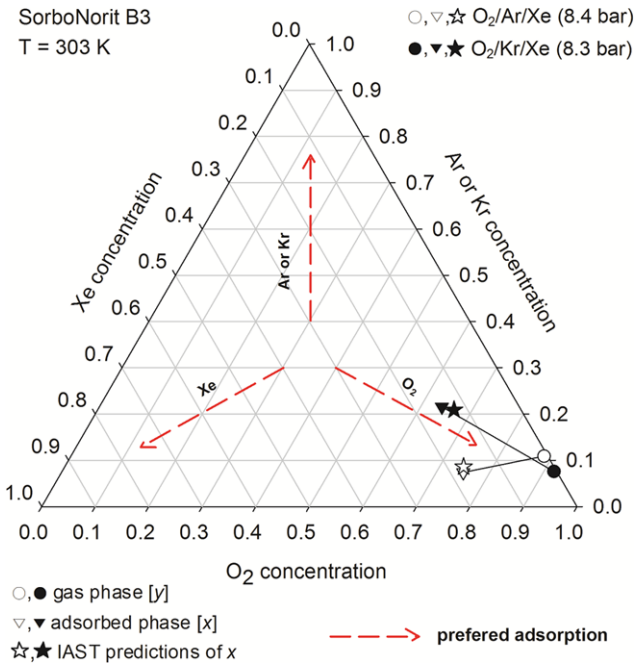

Fig. 10 Ternary diagram for adsorption of O_2/Ar/Xe and O_2/Kr/Xe on AC SorboNorit B3 at 303 K

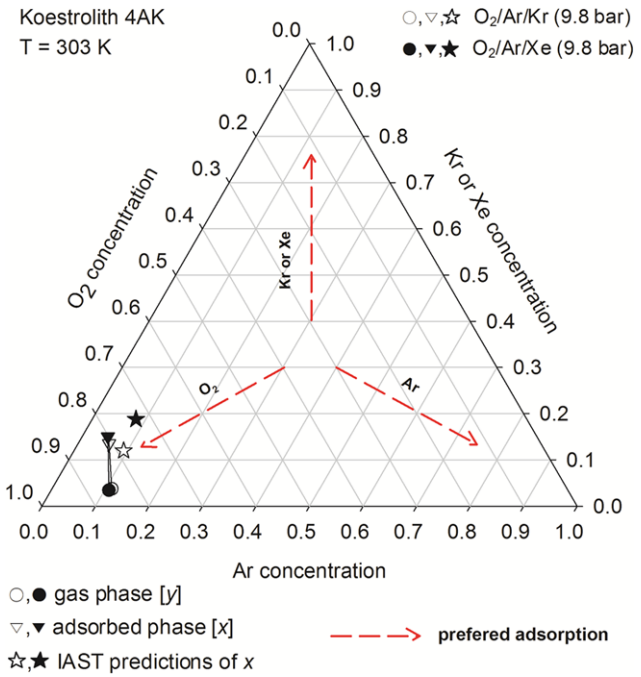

Fig. 11 Ternary diagram for adsorption of O_2/Ar/Kr and O_2/Ar/Xe on zeolite Koestrolith 4AK at 303 K

IAST predictions were somehow inaccurate, especially for the mixture containing Xe. This might be again an indication of unsatisfactory description of the isotherms data by the Langmuir model, since only a small amount of experimental points for xenon on Koestrolith 4AK are available (Fig. 2).

Those experimental ternary data meet the expectations that one can make about the selectivity of the gases just observing the single component adsorption isotherms. This observation implies that no significant interactions between species are found in the studied systems.

6 Conclusions

This work has presented series of experimental data on single component, binary and ternary adsorption equilibria of noble gases (Ar, Kr and Xe) and O_2 in one activated carbon sample (SorboNorit B3) and two zeolites (Koestrolith 13X-K2 and Koestrolith 4AK). All of the samples have shown qualitatively similar adsorption capacities. Xe was the most adsorbed gas, followed by Kr, then O_2 and Ar, which corresponds to the expected behavior of the adsorption of supercritical fluids at lower pressures. The adsorption capacity of all studied gases was found to be proportional to their critical temperatures.

AC SorboNorit B3 revealed higher affinity with Ar and O_2 in comparison with the zeolites. In the case of Kr, the carbon exhibits higher adsorbed amounts at pressures up to ca. 12 bar. For higher pressures the higher polarity of zeolite Koestrolith 13X-K2 surface appears to influence the polarization of Kr molecules, achieving higher adsorption capacities. Koestrolith 13X-K2 was also the best sample for adsorption of Xe in this study. This could be explained by the sample's favorable textural characteristics and the polarizability of Xe. The zeolite Koestrolith 4AK presented much smaller pore sizes and lower specific surface area compared to the other samples, which explain the lower adsorption capacities.

Experiments on binary mixtures confirmed the challenge of separating Ar/O_2 due to their very similar physical-chemical properties. Binary measurements with Kr/Xe have shown better results than simulations with new materials reported in literature, but more investigations on new materials are also desirable to improve the selectivity.

Ternary data confirmed the preferential adsorption of Xe over the other gases as well as of Kr over O_2 and Ar. Those experiments are also evidence for the absence of significant interactions between molecules of the different gases on the adsorption of their mixtures.

Predictions with the IAST model were generally satisfactory. The mismatching between experiment and model prediction found in some cases are attributed to inadequate description pure component data by the Langmuir isotherm model.

Acknowledgements The authors acknowledge financial support from Conselho Nacional de Desenvolvimento Científico e Tecnológico —CNPq (Brazil), Deutscher Akademischer Austausch Dienst—DAAD (Germany), Chemiewerk Bad Koestritz—CWK (Germany) and The Norit Group (The Netherlands).

References

Ansón, A., Kuznicki, S.M., Kuznicki, T., Haastrup, T., Wang, Y., Lin, C.C.H., Sawada, J.A., Eyring, E.M., Hunter, D.: Adsorption of argon, oxygen, and nitrogen on silver exchanged ETS-10 molecular sieve. Microporous Mesoporous Mater., **109**, 577–580 (2008)

Bastos-Neto, M., Torres, A.E.B., Azevedo, D.C.S., Cavalcante, C.L., Jr.: Methane adsorption storage using microporous carbons obtained from coconut shells. Adsorpt., J. Int. Adsorpt. Soc. **11**, 911–915 (2005)

Bastos-Neto, M., Canabrava, D.V., Torres, A.E.B., Rodriguez-Castellón, E., Jiménez-López, A., Azevedo, D.C.S., Cavalcante, C.L., Jr.: Effects of textural and surface characteristics of microporous activated carbons on the methane adsorption capacity at high pressures. Appl. Surf. Sci. **253**, 5721–5725 (2007)

Bazan, R.E., Bastos-Neto, M., Staudt, R., Papp, H., Azevedo, D.C.S., Cavalcante, C.L., Jr.: Adsorption equilibria of natural gas components on activated carbon: pure and mixed gas isotherms. Adsorp. Sci. Technol., **26**(5), 323–332 (2008)

Bondi, A.: van der Waals volumes and radii. J. Phys. Chem., **68**(3), 441–451 (1964)

Da Silva, J.L.F., Stampfl, C.: Trends in adsorption of noble gases He, Ne, Ar, Kr, and Xe on Pd(111)($\sqrt{3}$X$\sqrt{3}$)R30°: all-electron density-functional calculations. Phys. Rev. B, **77**, 1–13 (2008), 045401

Do, D.D.: Adsorption Analysis: Equilibria and Kinetics. Series on Chemical Engineering, vol. 2. Imperial College Press, London (1998). ISBN: 1-86094-130-3

Do, D.D., Do, H.D.: Adsorption of supercritical fluids in non-porous and porous carbons: analysis of adsorbed phase volume and density. Carbon **41**(9), 1777–1791 (2003)

Dobrinski, P., Krakau, G., Vogel, A.: Physik für Ingenieure. Teubner, Leipzig (2003). ISBN-10: 3-519-46501-9, ISBN-13: 97835194650110

Dreisbach, F.: Untersuchung von Adsorptionsgleichgewichten methanhaltiger Gasgemische an Aktivkohle als Grundlage zur Auslegung technischer Adsorptionsanlagen. PhD Thesis, Fortsch.—Ber. VDI, Reihe 3 Nr. 547. VDI Verlag, Düsseldorf (1998)

Dreisbach, F., Staudt, R., Keller, J.U.: High pressure adsorption data of methane, nitrogen, carbon dioxide and their binary and ternary mixtures on activated carbon. Adsorpt., J. Int. Adsorpt. Soc. **5**, 215–227 (1999)

Dreisbach, F., Lösch, H.W., Harting, P.: Highest pressure adsorption equilibria data: measurement with magnetic suspension balance and analysis with a new adsorbent/adsorbate-volume. Adsorpt., J. Int. Adsorpt. Soc., **8**(2), 95–109 (2002)

Fomkin, A.A., Serpinskii, V.V., Bering, B.P.: Investigation of the adsorption of xenon on NaX zeolite within a broad range of pressures and temperatures. Russian Chemical Bulletin. Translated from Izvestiya Akademii Nauk SSSR, Seriya Khimieheskaya **6**, 1244–1248 (1975)

Greathouse, J.A., Kinnibrugh, T.L., Allendorf, M.D.: Adsorption and separation of noble gases by IRMOF-1: grand canonical Monte Carlo simulations. Ind. Eng. Chem. Res., **48**(7), 3425–3431 (2009)

Herbst, A., Harting, P.: Thermodynamic description of excess isotherms in high-pressure adsorption of methane, Argon and nitrogen. Adsorpt., J. Int. Adsorpt. Soc. **8**, 111–123 (2002)

Hettema, H., Wormer, P.E.S., Jørgensen, P., Jensen, H.J.Aa., Helgaker, T.: Frequency-dependent polarizabilities of O_2 and van der Waals coefficients of dimers containing O_2. J. Chem. Phys., **100**(2), 1297–1302 (1994)

ISO 9277: Determination of the specific surface area of solids by gas adsorption using the BET method (1995)

Jee, J.G., Park, M.K., Yoo, H.K., Lee, K., Lee, C.H.: Adsorption and desorption characteristics of air on zeolite 5a, 10x, and 13x fixed beds. Sep. Sci. Technol., **37**(15), 3465–3490 (2002)

Jin, X., Malek, A., Farooq, S.: Production of argon from an oxygen-argon mixture by pressure swing adsorption. Ind. Eng. Chem. Res. **45**, 5775–5787 (2006)

Keller, J., Staudt, R.: Gas Adsorption Equilibria: Experimental Methods and Adsorption Isotherms. Springer, New York (2005). ISBN: 0-387-23597-3

Lemmon, E.W., Span, R.: Short fundamental equations of state for 20 industrial fluids. J. Chem. Eng. Data, **51**(3), 785–850 (2006)

Lowell, S., Shields, J.E., Thomas, M.A., Thommes, M.: Characterization of Porous Solids and Powders: Surface Area, Porosity and Density. Particle Technology Series. Springer, The Netherlands (2006). ISBN: 1-4020-2302-2

Mahajan, O.P., Walker, P.L., Jr.: Krypton adsorption on microporous carbons and 5A zeolite. J. Colloid Interface Sci., **29**(1), 129–137 (1969)

Marrocchi, Y., Razafitianamaharavo, A., Michot, L.J., Marty, B.: Low-pressure adsorption of Ar, Kr, and Xe on carbonaceous materials (kerogen and carbon blacks), ferrihydrite, and montmorillonite: Implications for the trapping of noble gases onto meteoritic matter. Geochim. Cosmochim. Acta, **69**(9), 2419–2430 (2005)

Mueller, U., Schubert, M., Teich, F., Puetter, H., Schierle-Arndt, K., Pastre, J.: Metal-organic frameworks—prospective industrial applications. J. Mater. Chem. **16**, 626 (2006)

Munakata, K., Kanjo, S., Yamatsuki, S., Koga, A., Ianovski, D.: Adsorption of noble gases on silver-mordenite. J. Nucl. Sci. Technol., **40**(9), 695–697 (2003)

Myers, A.L., Prausnitz, J.M.: Thermodynamics of mixed-gas adsorption. AIChE J., **11**(1), 121–126 (1965)

Pershina, V., Borschevsky, A., Eliav, E., Kaldor, U.: Adsorption of inert gases including element 118 on noble metal and inert surfaces from *ab initio* Dirac–Coulomb atomic calculations. J. Chem. Phys. **129**, 144106 (2008)

Reid, R.C., Prausnitz, J.M., Poling, B.E.: The Properties of Gases and Liquids, 4th edn. McGraw–Hill, New York (1987). ISBN: 0-07-051799-1

Rege, S.U., Yang, R.T.: Kinetic separation of oxygen and argon using molecular sieve carbon. Adsorpt., J. Int. Adsorpt. Soc. **6**, 15–22 (2000)

Rouquerol, F., Rouquerol, J., Sing, K.: Adsorption by Powders & Porous Solids. Academic Press, San Diego (1999). ISBN: 0-12-598920-2

Sandler, S.I.: Chemical and Engineering Thermodynamics., 3rd edn. Willey, New York (1999). ISBN: 0-471-18210-9

Schmidt, R., Wagner, W.: A new form of the equation of state for pure substances and its application to oxygen. Fluid Phase Equilib. **19**, 175–200 (1985)

Simonyan, V.V., Johnson, J.K., Kuznetsova, A., Yates, J.T., Jr.: Molecular simulation of xenon adsorption on single-walled. J. Chem. Phys., **114**(9), 4180–4185 (2001)

Staudt, R., Bohn, S., Dreisbach, F., Keller, J.U.: Gravimetric and volumetric measurements of helium adsorption equilibria on different porous solids. In: McEnaney, B., et al. (eds.) Characterization of Porous Solids 4, pp. 261–266. Royal Society of Chemistry, London (1997)

Talu, O.: Needs, status, techniques and problems with binary gas adsorption experiments. Adv. Colloid Interface Sci. **76–77**, 227–269 (1998)

Tegeler, Ch., Span, R., Wagner, W.: A new equation of state for argon covering the fluid region for temperatures from the melting line to 700 K at pressures up to 1000 MPa. J. Phys. Chem. Ref. Data, **28**(3), 779–850 (1999)

The Linde Group: Cryogenic Air Separation: History and Technological Progress. http://linde-anlagenbau.de/process_plants/air_separation_plants/documents/L_2_1_e_09_150dpi.pdf. Accessed 25 November 2009